NHR-8 regulated P-glycoproteins uncouple xenobiotic stress resistance from longevity in chemosensory *C. elegans* mutants

Gabriel A. Guerrero[1 †], Maxime J. Derisbourg[1†*], Laura E. Wester[1], Marco Gordia[1], J. Eike Dinort[1], María J. Alonso[1], Matías D. Hartman[1], Klara Schilling[1], Felix A.M.C. Mayr[1], Ryan J. Lu[4], Bérénice A. Benayoun[4] & Martin S. Denzel[1,2,3*]

[1]Max Planck Institute for Biology of Ageing
Joseph-Stelzmann-Str. 9b
D-50931 Cologne, Germany

[2]CECAD - Cluster of Excellence
University of Cologne
Joseph-Stelzmann-Str. 26
D-50931 Cologne, Germany

[3]Center for Molecular Medicine Cologne (CMMC)
University of Cologne
Robert-Koch-Str. 21
D-50931 Cologne, Germany

[4]Leonard Davis School of Gerontology
University of Southern California
Los Angeles, CA 90089, USA

[†]These authors contributed equally

*correspondence: mdenzel@age.mpg.de and mderisbourg@age.mpg.de

Abstract

Longevity is often associated with stress resistance, but whether they are causally linked is incompletely understood. Here we investigate chemosensory defective *Caenorhabditis elegans* mutants that are long-lived and stress resistant. We find that mutants in the intraflagellar transport protein gene *osm-3* were significantly protected from tunicamycin-induced ER stress. While *osm-3* lifespan extension is dependent on the key longevity factor DAF-16/FOXO, tunicamycin resistance was not. *osm-3* mutants are protected from bacterial pathogens, which is *pmk-1* p38 MAP kinase dependent while TM resistance was *pmk-1* independent. Expression of P-glycoprotein (PGP) xenobiotic detoxification genes was elevated in *osm-3* mutants and their knockdown or inhibition with verapamil suppressed tunicamycin resistance. The nuclear hormone receptor *nhr-8* was necessary to regulate PGPs and tunicamycin resistance in a cholesterol-dependent fashion. We thus identify a cell-nonautonomous regulation of xenobiotic detoxification and show that separate pathways are engaged to mediate longevity, pathogen resistance, and xenobiotic detoxification in *osm-3* mutants.

38 **Introduction**

39 Chemosensation is a genetically tractable phenotype in various model organisms. In
40 *C. elegans*, many mutants with defective chemosensation have been identified.
41 Sensory phenotypes are complex in nature and many of the classical chemosensory
42 mutants were originally characterized by their behavioral phenotypes. Odr mutants for
43 example have an abnormal odorant response while Osm (osmotic avoidance
44 abnormal) mutants do not avoid high salt environments (Bargmann, 2006). Mutations
45 in components of neuronal G-protein coupled receptor (GPCR) signaling, such as *tax-4*
46 and *odr-1,* cause atypical chemosensory behavior (Bargmann, 2006). These mutants
47 are not only characterized by a failure to adequately respond to their environment, but
48 show additional phenotypes linked to various life traits including pathogen resistance,
49 increased lifespan, and drug detoxification (Gaglia et al., 2012, Apfeld and Kenyon,
50 1999, Dent et al., 2000). Many chemosensory mutants are long-lived and this
51 phenotype depends on the DAF-16/FOXO transcription factor that is regulated by the
52 insulin signaling pathway (Apfeld and Kenyon, 1999).

53 Beyond mutations in GPCRs, variants in genes involved in the development of amphid
54 sensory neurons can lead to chemosensory defects. One example are mutations in
55 intraflagellar transport (IFT) proteins that prevent full cilia development of amphid
56 sensory neurons (Inglis et al., 2007). Alterations in the IFT genes *osm-3* and *daf-10*
57 disrupt the development of neuronal dendrites that project toward the tip of the nose,
58 where they are exposed to the outer environment (Inglis et al., 2007). Thus, IFT
59 mutants are usually characterized by defects in the chemical perception of their
60 environment. Further, developmental defects in lumen formation of the amphid head
61 channel in *daf-6* mutants prevent the direct contact of amphid sensory neurons with
62 the outside (Perens and Shaham, 2005), resulting in chemosensory defects.

63 In wild type (WT) worms, amphid and phasmid sensory neurons can be visualized
64 using the lipophilic dye DiI (1,1'-dioctadecyl-3,3,3',3'-tetramethylindocarbocyanine
65 perchlorate), which fluorescently stains them bright red. The dye is passively taken up
66 by sensory neurons when they are fully developed and in contact with the environment.
67 Dye filling defective (Dyf) *C. elegans* are defined by an inability to take up DiI into their
68 sensory neurons (Inglis et al., 2007). The Dyf phenotype arises in *daf-6* animals and
69 also in many IFT mutants. Interestingly, Dyf mutants have unique stress resistance
70 phenotypes that act via different signaling pathways. One such Dyf mutant,
71 *daf-10(m79)*, has a unique resistance to pathogenic bacteria that was proposed to be
72 downstream of sensory input (Gaglia et al., 2012). Further, pairs of amphid head
73 neurons, such as ASH and ASJ that often become disrupted in Dyf mutants help
74 coordinate the innate immune response to bacterial stress after infection (Meisel et al.,
75 2014). Longevity is often associated with activation of physiological stress response
76 pathways and has been shown to be regulated by the insulin signaling pathway in Dyf
77 *C. elegans* (Apfeld and Kenyon, 1999).
78 Conserved mechanisms of longevity and stress resistance have additionally been
79 linked to hyposmia in higher model organisms. In *Drosophila melanogaster*, loss of the
80 putative chemoreceptor *Or83b* has been shown to significantly increase lifespan
81 (Libert et al., 2007). Further, mice with ablated olfactory sensory neurons, have a
82 unique metabolic signature that protects them from high-fat diets (Riera et al., 2017).
83 While the olfactory machinery is seemingly more complex in higher organisms,
84 *C. elegans* have unique phenotypes associated with the loss or alteration of their
85 sensory neurons. First, unbiased screens for drug resistance have independently
86 identified the Dyf phenotype as a common feature in drug resistant *C. elegans* (Fujii et
87 al., 2004, Menez et al., 2016, Collins et al., 2008). Selection for resistance to the
88 anthelmintic drug ivermectin was shown to enrich for Dyf mutants in several forward

89 genetic screens (Menez et al., 2016, Page, 2018, Dent et al., 2000). Follow-up work
90 identified P-glycoproteins (PGPs), a class of ATP binding cassette (ABC) transporters,
91 as the drivers behind ivermectin resistance in Dyf mutants (Ardelli and Prichard, 2013).
92 Second, some chemosensory mutations, such as in *daf-10*, lead to resistance to
93 pathogenic bacteria (Gaglia et al., 2012).
94 Here, we characterize a long-lived Dyf mutant, *osm-3*, that was previously identified in
95 a forward genetic screen for resistance to the potent ER stressor tunicamycin (TM).
96 From this screen, we reported the role of the hexosamine biosynthetic pathway in TM
97 resistance and longevity (Denzel et al., 2014). Our aim was to uncover the mechanism
98 by which Dyf mutants are resistant to TM. We found that the TM resistance of *osm-3*
99 mutants is independent from its longevity and pathogen resistance phenotypes.
100 Further, we showed that PGPs mediate TM resistance in Dyf animals and we found
101 that the nuclear hormone receptor *nhr-8* mediates *osm-3* drug resistance. The “Green
102 Theory” of aging proposes that the accumulation of toxic endo- and xenobiotic debris
103 contributes to physiological decline with age (Afschar et al., 2016, Gems and McElwee,
104 2005). Our work highlights drug resistance as a unique characteristic of Dyf mutants
105 and functionally uncouples it from known stress response pathways that have been
106 implicated in stress resistance and longevity of chemosensory mutants.

107 **Results**

108 **Dye filling defective *C. elegans* mutants are resistant to TM**

109 Tunicamycin (TM) is commonly used to induce endoplasmic reticulum (ER) stress by
110 inhibiting the addition of N-glycans to nascent polypeptides (Parodi, 2000, Heifetz et
111 al., 1979). In *C. elegans*, where the ER machinery is conserved, treatment with TM is
112 toxic and induces the ER unfolded protein response. In fact, on plates containing TM
113 at concentrations above 4 µg/mL, newly hatched larvae die at early developmental
114 stages (Shen et al., 2001). Previously, we had carried out an ethyl methane-sulfonate
115 mutagenesis screen to identify long-lived mutants using TM resistance in *C. elegans*
116 as a proxy phenotype for longevity (Denzel et al., 2014). The largest cohort of
117 classifiable mutants presented the Dyf phenotype (Figure 1A).

118 Among the Dyf mutants from the TM resistance screen, we found new alleles of genes
119 previously linked to ciliary development. The mutant allele we selected for our
120 investigation, *osm-3(dh441)IV* (this allele will be referred to hereafter as *osm-3*),
121 carries a premature stop in the eighth exon, which prevents normal cilia development
122 causing the Dyf phenotype (Figure 1A, Figure 1B). *osm-3* is a member of the kinesin
123 family involved in axonal development and transport, and mutants are known to show
124 a Dyf phenotype (Inglis et al., 2007). While WT worms fail to develop on TM at
125 concentrations above 4 µg/mL, *osm-3* mutants fully develop at concentrations at least
126 up to 10 µg/mL TM (Figure 1C). Loss of *osm-3,* as well as other Dyf mutations, promote
127 longevity in *C. elegans* (Apfeld and Kenyon, 1999). Demographic lifespan analysis of
128 *osm-3* indeed confirmed extended lifespan in our point mutant (Figure 1D and
129 Supplementary Table 1). *osm-3* mutants, and Dyf mutants in general, have never been
130 described as TM resistant especially at concentrations as high as 10 µg/mL.

131 To further explore whether the Dyf phenotype is linked to TM resistance, we tested
132 other Dyf mutants that were previously described as long-lived (Apfeld and Kenyon,

133 1999). To our surprise, all long-lived Dyf mutants that we tested proved to be
134 significantly TM resistant at the WT lethal dose of 10 µg/mL TM (Figure 1E, Figure 1-
135 figure supplement 1A-G). In contrast, the long-lived chemosensory *odr-1(n1936)X*,
136 *odr-3(n2150)V,* and *tax-4(p678)III* mutants that do not display a Dyf phenotype were
137 only slightly TM resistant (Figure 1E, Figure 1-figure supplement 1J-I). Our data thus
138 suggest that, among the larger class of chemosensory defective mutants, lifespan
139 extension is uncoupled from TM resistance.

140 **ER stress response is blunted in *osm-3* mutants**

141 TM treatment activates the ER unfolded protein response (UPR^{ER}); we thus
142 characterized the overall transcriptional response of *osm-3* mutants upon TM
143 treatment. We performed transcriptomic analyses of *osm-3* and WT worms after
144 6 hours of TM treatment. Notably, the gene ontology (GO) terms related to ER stress
145 and ER protein folding showed significant upregulation in WT animals, but not in *osm-3*
146 mutants (Figure 2A). RT-qPCR analysis of UPR target genes further confirmed that
147 there was no UPR^{ER} induction in TM-treated *osm-3* mutants compared to the WT
148 (Figure 2-figure supplement 1). A hallmark of UPR^{ER} activation in *C. elegans* is the
149 upregulation of the molecular chaperone HSP-4/BiP (Shen et al., 2001). Upon TM
150 treatment of *osm-3* mutants carrying an *hsp-4*::GFP reporter construct, there was no
151 significant increase in the GFP signal compared to the untreated control, while in the
152 WT the GFP levels were significantly increased (Figure 2B,C). This observation
153 corroborates the results from the transcriptome analysis.

154 One potential explanation for a suppressed UPR^{ER} response in *osm-3* mutants might
155 be a general defect in the stress signaling pathway. To address this possibility, we
156 sought to activate the UPR by alternate means. The ER membrane protein
157 SEL-1/HRD3 is a cofactor of the HRD1 ubiquitin ligase complex involved in ER-

158 associated degradation (ERAD)(Hampton et al., 1996). Using *sel-1* RNAi to inhibit
159 ERAD, we observed a robust activation of the *hsp-4*::GFP reporter, suggesting a
160 functional UPR^{ER} response upon ER stress in *osm-3* mutants (Figure 2D,E). We
161 further used DTT treatment to induce ER stress and found normal levels of *hsp-4*::GFP
162 induction and *xbp-1* splicing (Figure 2F) in *osm-3* mutants. Together, these
163 observations rule out that the reduced response to TM observed in *osm-3* mutants was
164 due to a defect in UPR signaling.

165 **TM resistance in *osm-3* mutants is independent from *daf-16* or the PMK-1/p38**
166 **MAPK pathway**

167 The lifespan extension observed in chemosensory defective *C. elegans* as well as in
168 *Drosophila* has been shown to be at least partially insulin signaling dependent (Apfeld
169 and Kenyon, 1999, Libert et al., 2007). Therefore, we performed a demographic
170 lifespan analysis to determine the role of the insulin signaling pathway in the lifespan
171 extension of *osm-3* mutants. Indeed, the *osm-3* lifespan extension was fully *daf-16*
172 dependent, as the lifespan of the *osm-3; daf-16* double mutants was identical to the
173 *daf-16* lifespan (Figure 3A, Supplementary Table 1). In stark difference to *osm-3*
174 survival, the *osm-3; daf-16* double mutant remained resistant to TM while *daf-16* single
175 mutants do not develop at 10 µg/mL TM (Figure 3B). A previous study by Henis-
176 Korenblit et al. had shown elevated *hsp-4*::GFP levels during *daf-16* knockdown in a
177 *daf-2* mutant (Henis-Korenblit et al., 2010). We therefore asked whether the
178 knockdown of *daf-16* would sensitize *osm-3* mutants to TM. Interestingly, knock-down
179 of *daf-16* by RNAi did not elevate the *hsp-4*::GFP response of *osm-3* mutants after TM
180 treatment (Figure 3-figure supplement 3A). Given the links between the insulin
181 signaling pathway and ER stress signaling (Henis-Korenblit et al., 2010, Kyriakakis et
182 al., 2017, Matai et al., 2019, Labbadia and Morimoto, 2014), we were further surprised

183 to find that *daf-2* mutants failed to develop on 10 µg/mL TM while *osm-3* mutants fully
184 developed (Figure 3-figure supplement 3B). Together, this evidence suggests that the
185 *osm-3* lifespan extension and TM drug resistance are uncoupled and appear to act via
186 independent or parallel pathways.

187 In *C. elegans, Pseudomonas aeruginosa* PA14 is a pathogen that is often used to
188 study innate immunity. The PMK-1 p38 mitogen-activated protein kinase (MAPK)
189 pathway as well as UPR^{ER} targets have been implicated in the innate immune
190 response of *C. elegans* during PA14 infection (Richardson et al., 2010, Haskins et al.,
191 2008). Given the role of ER homeostasis in innate immunity and the TM resistance of
192 *osm-3* mutants, we speculated that they would be more robust on PA14 than WT.
193 Indeed, *osm-3* mutants were resistant to PA14, and this increased pathogen resistance
194 was lost upon *pmk-1* knockdown (Figure 3C). With this in mind, we tested whether
195 *pmk-1* mutation could suppress the *osm-3* TM resistance. The *osm-3; pmk-1* double
196 mutant was fully resistant to TM, while the *pmk-1* single was sensitive (Figure 3D),
197 demonstrating that TM resistance and *pmk-1* mediated pathogen resistance are
198 uncoupled in *osm-3* mutants. Taken together, insulin signaling and the MAPK pathway,
199 two major stress response pathways in *C. elegans* that have links to ER protein quality
200 control, are not required for TM resistance in *osm-3* mutants.

201 **NHR-8 and PGPs regulate xenobiotic detoxification and TM resistance in *osm-3***
202 **mutants**

203 Given the absence of ER stress in TM-treated *osm-3* mutants along with the genetic
204 separation of TM resistance from insulin or MAPK signaling, we hypothesized that TM
205 might be cleared from worm tissues through xenobiotic detoxification. PGPs are a
206 conserved family of ATP binding cassette (ABC) transporters found on the cell
207 membrane (Sangster, 1994) involved in toxin clearance, and *C. elegans* have 15 *pgp*

208 genes. Using quantitative PCR, we found a significant upregulation of *pgp-3*, *pgp-5*,
209 *pgp-11*, and *pgp-13* in *osm-3* mutants (Figure 4A). The nuclear hormone receptor
210 NHR-8 has been linked to xenobiotic detoxification and *pgp* regulation in *C. elegans*
211 (Menez et al., 2019, Lindblom et al., 2001). Indeed, we found that the upregulation of
212 *pgp* expression in *osm-3* mutants was suppressed in the *osm-3; nhr-8* double mutant
213 (Figure 4A). PGP upregulation suggested a role for PGPs in the TM resistance of
214 *osm-3* mutants. Therefore, we tested if RNAi-mediated PGP knock-down in *osm-3*
215 mutants would suppress TM resistance. We focused on the upregulated *pgp-5*, *pgp-11*
216 and *pgp-13,* and on *pgp-8 and pgp-12*. Interestingly, knock-down of *pgp-5, pgp-11*,
217 and *pgp-12* partially reduced the TM resistance of the *osm-3* mutants (Figure 4B).
218 Next, we used verapamil to inhibit PGPs. Verapamil has been used to specifically
219 inhibit PGP activity, re-sensitizing worms to the anthelmintic compound ivermectin
220 (Menez et al., 2016). Indeed, 1 nM verapamil significantly suppressed development of
221 *osm-3 C. elegans* in the presence of TM, showing no effect on controls without TM
222 (Figure 4C). These partial effects likely suggest that xenobiotic detoxification is
223 achieved by multiple PGPs which are transcriptionally orchestrated by *nhr-8*. This led
224 us to ask whether *osm-3* TM resistance was dependent on NHR-8. Strikingly, the
225 developmental TM assay revealed that the resistance of *osm-3* mutants was largely
226 suppressed in the *osm-3; nhr-8(hd117)IV* double mutant (Figure 4D), suggesting that
227 NHR-8 is necessary for *osm-3* TM resistance. As suggested by a role of PGPs in
228 ivermectin resistance, we found that *osm-3* mutants fully developed to adults in the
229 presence of 6 µg/mL ivermectin that is lethal to WT animals (Figure 4E). Ivermectin
230 resistance of *osm-3* mutants was suppressed by loss of NHR-8. Dyf *C. elegans*
231 mutants have been independently identified in drug resistance screens (Fujii et al.,
232 2004, Menez et al., 2016, Dent et al., 2000). Consistent with these findings, we
233 observed that *osm-3* mutants were resistant to 200 nM paraquat, as they fully develop

234 at a concentration that is toxic to WT *C. elegans* (Figure 4F). Consistent with a role in
235 xenobiotic detoxification, NHR-8 was required for the paraquat resistance of the *osm-3*
236 mutants (Figure 4F).
237 We next reasoned that resistance of *osm-3* mutants should be limited to chemical
238 stressors that can be eliminated by xenobiotic detoxification. We thus tested heat
239 stress and hydrogen peroxide (H_2O_2) induced oxidative stress. Paraquat and hydrogen
240 peroxide are both oxidative stressors, but paraquat acts indirectly via the mitochondria
241 (Castello et al., 2007) while hydrogen peroxide is a primary cause for oxidative
242 damage. When challenged with heat or hydrogen peroxide, *osm-3* mutants showed no
243 difference to WT animals, suggesting that *osm-3* mutants are not resistant to these
244 non-xenobiotic stressors (Figure 4-figure supplement 1A,B).
245 Given the involvement of PGP-dependent xenobiotic detoxification in TM resistance of
246 *osm-3* mutants, we wondered about its role in the longevity of *osm-3* mutants. Notably,
247 verapamil did not shorten *osm-3* lifespan (Figure 4G). Moreover, verapamil did not
248 affect WT lifespan (Figure 4G and Supplementary Table 1) and had no visible effect
249 on WT development (Figure 4-figure supplement 1C). Finally, we asked about a role
250 of NHR-8 in *osm-3* longevity. While *nhr-8* mutation shortens lifespan, the *osm-3*
251 mutation extended both WT and *nhr-8* survival to a similar degree (Figure 4H).
252 Together, these data support the conclusion that the xenobiotic stress resistance and
253 longevity phenotypes of *osm-3* mutants are mediated by independent pathways.

254 **Sterol signals modulate TM resistance**

255 We aimed to further understand the systemic signals that control xenobiotic
256 detoxification of TM. The NHR-8 ligand remains unknown, but is likely a sterol molecule
257 derived from cholesterol metabolism (Magner et al., 2013). We thus tested the role of
258 cholesterol in TM resistance and found that omitting cholesterol from the culture plate

259 for one generation leads to TM hypersensitivity in both WT and *osm-3* animals
260 (Figure 5A). To specifically assess a role of cholesterol-derived signals in TM
261 resistance, we used the *hsp-4*::GFP reporter and found that high cholesterol
262 significantly reduced TM-induced ER stress (Figure 5B). Developmental cholesterol
263 dose response assays in the presence of TM confirmed that WT TM resistance is
264 cholesterol dependent. In *nhr-8* and *osm-3; nhr-8* double mutants, however,
265 cholesterol treatment failed to protect from TM toxicity (Figure 5C). This demonstrates
266 a key role of NHR-8 in mediating TM resistance downstream from sterol signals. These
267 observations together suggest cell-nonautonomous regulation of xenobiotic
268 detoxification of TM by cholesterol-derived ligands that enhance PGP expression via
269 NHR-8.

270 **Discussion**

271 In this study, we found that *osm-3* mutants as well as other long-lived Dyf mutants are
272 resistant to the ER toxin TM. Instead of an activated stress signaling status that might
273 explain the TM resistance, *osm-3* Dyf mutants show no UPR^{ER} induction upon TM
274 treatment. Consistent with previous findings (Apfeld and Kenyon, 1999) the lifespan
275 extension of *osm-3* was *daf-16* dependent. Despite the established link between the
276 insulin signaling pathway and stress resistance, the TM resistance in *osm-3* mutants
277 was not insulin signaling dependent. Further, *osm-3* mutants were pathogen resistant
278 and this resistance was fully dependent on the PMK-1/p38 MAPK pathway. We were
279 surprised that neither of the two pathways weakened the TM resistance phenotype.
280 Dyf *C. elegans* drug resistance is not specific to TM, as we also observed resistance
281 to paraquat and ivermectin. While paraquat and ivermectin resistance have been
282 previously reported in Dyf mutants (Dent et al., 2000, Fujii et al., 2004, Menez et al.,
283 2016), no studies have demonstrated similar resistance mechanisms in Dyf *C. elegans*
284 mutants to TM. Our findings show that drug resistance is due to increased PGP
285 expression in Dyf worms, suggesting a causal role of xenobiotic detoxification in the
286 drug resistance phenotype. Importantly, we demonstrate regulation of PGPs by the
287 nuclear hormone receptor NHR-8. Genetic or pharmacological PGP inhibition, as well
288 as loss of *nhr-8* significantly re-sensitized *osm-3* mutants to TM, ivermectin, and
289 paraquat. Potential NHR-8 ligands are derived from cholesterol (Magner et al., 2013)
290 and we observed that WT development on lower TM concentrations was strongly
291 cholesterol and NHR-8 dependent.

292 Given that improved protein homeostasis is one of the cellular hallmarks of longevity
293 (Lopez-Otin et al., 2013), we presumed that selection for TM resistance would serve
294 as a proxy phenotype for longevity given that TM specifically targets ER protein folding.
295 More specifically, we expected that high fidelity ER protein quality control would be the

296 driver of longevity in these mutants. Previous findings describing increased
297 hexosamine biosynthetic pathway flux (Denzel et al., 2014) or constitutive XBP-1
298 activation (Taylor and Dillin, 2013) have linked protein homeostasis to longevity and
299 stress resistance (Denzel and Antebi, 2015); therefore the connection between TM
300 resistance and longevity seemed apparent. Given that Dyf mutants are resistant to
301 pathogenic bacteria through enhanced ER homeostasis, we also speculated that TM
302 resistance might serve as a proxy phenotype for pathogen resistance. On the contrary,
303 we found that TM resistance is a consequence of xenobiotic detoxification via PGPs,
304 and NHR-8 regulated control of PGPs was not involved in the longevity of *osm-3*
305 mutants. *pmk-1* and *daf-16* were required for pathogen resistance and longevity,
306 respectively, but not for the drug resistance of *osm-3* mutants. Together, these findings
307 demonstrate that the three phenotypes of *osm-3* mutants (i.e. xenobiotic resistance,
308 longevity, and protection from pathogens) are independent and controlled by
309 separable genetic pathways. Our observations thus support a model in which the
310 chemosensation defect activates a number of parallel pathways that are responsible
311 for the distinct phenotypes of *osm-3* mutants.
312 Adding another dimension to the cell-nonautonomous regulation of innate immunity
313 (Aballay, 2013), we propose that the nervous system regulates systemic xenobiotic
314 detoxification in *C. elegans*, likely through a sterol ligand. Our data suggest that
315 mutants with defective amphid neurons have increased PGP expression. Several
316 PGPs have been shown to be expressed in non-neuronal tissue (Lincke et al., 1993,
317 Sheps et al., 2004). Moreover, we found that PGP expression is regulated by *nhr-8*,
318 which has also been shown to be expressed in the intestine of *C. elegans* (Magner et
319 al., 2013). Combining this previous information with our finding that Dyf mutants are
320 resistant to several uniquely toxic drugs, we conclude that neuronal signaling controls
321 drug resistance through nuclear hormone signaling. Given our observation that

322 supplementation with cholesterol is itself sufficient for TM resistance in WT worms one
323 might further investigate the link between neuronal states and the specific cholesterol-
324 derived signal that drives these drug resistance phenotypes.
325 PGPs are likely regulated in *C. elegans* to help them combat toxins found in their
326 natural habitat. Toxic metabolites are undoubtedly common in the soil where
327 *C. elegans* are found. The drugs used in our study, ivermectin (a derivative of
328 avermectin) (Burg et al., 1979) and TM, were first discovered as antibiotics that are
329 produced by soil bacteria (Takatsuki et al., 1971). Because *C. elegans* have no
330 adaptive immune response, having PGPs as part of their innate immune system allows
331 them to clear toxic molecules they may encounter in the wild. While Dyf mutants do
332 not occur in the wild, our data nonetheless demonstrate a link between environmental
333 sensing and drug resistance.
334 In humans, PGPs have been implicated in drug resistant malignancies (Lehne, 2000).
335 Using *C. elegans* as a tool to study the cross talk between tissues, one might be able
336 to better understand how extracellular signaling drives ABC transporter expression in
337 chemotherapy resistant cancer. Further studies in cell culture might also characterize
338 TM, as well as other toxic metabolites, as substrates for *C. elegans* PGPs.

339 **Materials and Methods**

Key Resources Table				
Reagent type (species) or resource	**Designation**	**Source or reference**	**Identifiers**	**Additional information**
strain, strain background (*E. coli*)	HT115 [*L4440::sel-1*]	Source Bioscience	CELE_F45D3.5	Ahringer RNAi library
strain, strain background (*E. coli*)	HT115 [*L4440::daf-16*]	Source Bioscience	CELE_R13H8.1	Ahringer RNAi library
strain, strain background (*E. coli*)	HT115 [*L4440::pgp-5*]	Source Bioscience	CELE_C05A9.1	Ahringer RNAi library
strain, strain background (*E. coli*)	HT115 [*L4440::pgp-8*]	Source Bioscience	CELE_T21E8.3	Ahringer RNAi library
strain, strain background (*E. coli*)	HT115 [*L4440::pgp11*]	Source Bioscience	CELE_DH11.3	Ahringer RNAi library
strain, strain background (*E. coli*)	HT115 [*L4440::pgp-12*]	Source Bioscience	CELE_F22E10.1	Ahringer RNAi library
strain, strain background (*E. coli*)	HT115 [*L4440::pgp-13*]	Source Bioscience	CELE_F22E10.2	Ahringer RNAi library
genetic reagent (*C. elegans*)	*osm-3(dh441)IV*	other	AA1962	available from A. Antebi or M.S. Denzel
genetic reagent (*C. elegans*)	*daf-16(mu86)I*	CGC	CF1038	
genetic reagent (*C. elegans*)	*pmk-1(km25)IV*	CGC	KU25	
genetic reagent (*C. elegans*)	*osm-3(dh441)IV; nhr-8(hd117)IV*	this paper	MSD420	available from M.S. Denzel
genetic reagent (*C. elegans*)	*osm-3(dh441)IV; daf-16(mu86)I*	this paper	MSD422	available from M.S. Denzel

genetic reagent (*C. elegans*)	*osm-3(dh441)IV; pmk-1(km25)IV*	this paper	MSD423	available from M.S. Denzel
genetic reagent (*C. elegans*)	*odr-1(n1936)X*	CGC	CX2065	
genetic reagent (*C. elegans*)	*odr-3(n2150)V*	CGC	CX2205	
genetic reagent (*C. elegans*)	*osm-6(p811)V*	CGC	PR811	
genetic reagent (*C. elegans*)	*tax-4(p678)III*	CGC	PR678	
genetic reagent (*C. elegans*)	*nhr-8(hd117)IV*	other	AA968	available from A. Antebi or M.S. Denzel
genetic reagent (*C. elegans*)	*N2; dhEx451(nhr-8::gfp; coel::RFP)*	CGC	AA1027	
genetic reagent (*C. elegans*)	*osm-3(dh441)IV; zcIs4 [hsp-4::GFP]V*	other	AA2774	available from A. Antebi or M.S. Denzel
genetic reagent (*C. elegans*)	*zcIs4[hsp-4::GFP]V*	CGC	SJ4005	
genetic reagent (*C. elegans*)	*che-11(e1810)V*	CGC	CB3330	
genetic reagent (*C. elegans*)	*daf-10(e1387)IV*	CGC	CB1387	
genetic reagent (*C. elegans*)	*osm-1(p808)X*	CGC	PR808	
genetic reagent (*C. elegans*)	*dyf-1(mn335)I*	CGC	SP1205	
genetic reagent (*C. elegans*)	*che-2(e1033)X*	CGC	CB1033	
genetic reagent (*C. elegans*)	*osm-5(p813)X*	CGC	PR813	
commercial assay or kit	Direct-zol RNA Microprep	Zymo Research	R2060	

commercial assay or kit	SMARTer Stranded RNA-Seq HT Kit	Takara	634838	
commercial assay or kit	Ribo-zero Gold kit	Illumina	MRZG12324	
chemical compound, drug	Tunicamycin	Calbiochem	CAS 11089-65-9	
chemical compound, drug	Dithiothreitol	Sigma Aldrich	CAS 3483-12-3	
chemical compound, drug	Methyl viologen dichloride hydrate	Sigma Aldrich	CAS 75365-73-0	Paraquat
chemical compound, drug	Ivermectin	Sigma Aldrich	CAS 70288-86-7	
chemical compound, drug	Verapamil hydrochloride	Sigma Aldrich	CAS 152-11-4	
chemical compound, drug	Cholesterol	Sigma Aldrich	CAS 57-88-5	
chemical compound, drug	1,1′-Dioctadecyl-3,3,3′,3′-tetramethylindocarbocyanine perchlorate	Sigma Aldrich	CAS 41085-99-8	DiI
software, algorithm	R statistical software	cran.r-project.org	DESeq2 1.16.1	PMID: 25516281
other	Reference Genome	ENSEMBL	WBCel235	

340

341 **Worm maintenance**

342 *C. elegans* nematodes were cultured using standard husbandry methods at 20°C on
343 nematode growth media (NGM) agar plates seeded with *E. coli* strain OP50 unless
344 otherwise stated (Brenner, 1974).

345 **Dye filling assay in *C. elegans***

346 The dye filling assay was performed on a synchronized population of day 1 adults. 40-
347 60 adult worms were placed in M9 containing 10 µg/mL DiI. They were left at room
348 temperature for two hours in the staining medium, then transferred to NGM plates

349 seeded with *E. coli* OP50. The worms were then allowed to crawl on the food for one
350 hour to allow for the dye to be cleared from the gut. The worms were scored for dye
351 filling using a Leica SPX-8 confocal microscope or a Leica fluorescent stereo-
352 microscope. Images were taken using the confocal microscope.

353 **Drug resistance assays**

354 NGM plates containing either TM, paraquat or ivermectin were used in developmental
355 assays to test for resistance. To this end, we performed a 4h egg lay on NGM plates
356 at room temperature then transferred the eggs to control and drug containing plates
357 and recorded the number of eggs per plate. After incubation for four days at 20°C,
358 plates were scored by counting the total number of L4 larvae or adults on each plate.
359 Paraquat plates were prepared by adding 1M methyl viologen dichloride (paraquat)
360 directly onto seeded NGM plates for a final concentration of 200 μM and allowed to dry
361 immediately before use. Ivermectin plates were prepared by adding ivermectin directly
362 to the NGM medium at a final concentration of 6 μg/mL before pouring the plates.
363 Modified NGM plates containing no cholesterol were made by using standard NGM
364 without the addition of cholesterol. NGM agar plates containing 5, 25 or 50 μg/mL
365 Cholesterol were used for development when specifically stated. These modified NGM
366 plates were then supplemented with drugs as described above. All of the drug
367 development assays were performed using *E. coli* OP50 or *E. coli* HT115 bacteria. For
368 the TM RNAi experiments (Figure 4B), animals were cultured for one generation on
369 *pgp-5*, *pgp-8, pgp-11, pgp-12* or *pgp-13* RNAi supplemented with DMSO. The offspring
370 was placed on RNAi plates supplemented with 10 μg/mL TM.

371 **ER stress quantification**

372 Synchronized day 1 adults were transferred to control and TM containing NGM plates
373 seeded with OP50. After 6 hours of stress induction *hsp-4*::GFP levels were measured

374 by large particle flow cytometry in both the WT and *osm-3(dh441)IV* background using
375 the Union Biometrica Biosorter and imaged using a Leica fluorescent stereo-
376 microscope. For RNAi experiments, animals were raised on control and *daf-16* or *sel-1*
377 RNAi. Synchronized day 1 adults were transferred to vehicle or TM containing plates
378 seeded with control or experimental RNAi. After 6 hours of stress, GFP levels were
379 measured using the Biosorter. GFP values were normalized to time of flight. At least
380 100 animals were analyzed per condition. For RNA isolation, day 1 adults were treated
381 with 10 mM DTT in S Basal buffer containing *E. coli* OP50 for 2 hours and then snap
382 frozen.

383 **Quantitative PCR**

384 For ER stress induction day 1 adults were washed from their plates and transferred to
385 either control or TM containing plates, where they were incubated for 6 hours. The
386 animals were then washed off using M9 and snap frozen in trizol. Unstressed
387 synchronized animals were collected at day 1 of adult hood for RNA extraction. RNA
388 was prepared using Zymo Research Direct-zol RNA Microprep kit. SYBR green was
389 used to perform quantitative PCR (RT-qPCR). See Supplementary Table 2 for list of
390 qPCR primers used in this study. Primer efficiency was tested and was always above
391 90%.

392 **Lifespan analysis**

393 Adult lifespan analysis was performed at 20°C on mutant and WT *C. elegans*. The
394 animals were synchronized in a four-hour egg lay. Animals were scored as dead or
395 alive every second day until the end of the experiment. Animals were transferred every
396 day for the first seven days. Statistical analysis on the Kaplan-Meier survival curves
397 was performed using Microsoft Excel. See Supplementary Table 1 for lifespan
398 statistics. Each survival experiment was performed at least twice.

399 **Hydrogen peroxide survival assay**

400 1M hydrogen peroxide (H_2O_2) was added to unseeded NGM plates to a final
401 concentration of 1 μM and allowed to dry for several minutes. Synchronized day one
402 adults were then transferred onto the plates and incubated at 25°C. The animals were
403 then scored every 2 hours for survival. 20 to 50 animals were used in each
404 experimental condition.

405 **Pathogenic bacteria survival assay**

406 The *Pseudomonas aeruginosa* strain PA14 was grown in LB media and seeded onto
407 high peptone NGM plates and incubated for 12 hours at 37°C immediately before the
408 start of the experiment. Day one animals were first transferred to unseeded NGM
409 plates to crawl around the plate and remove any excess *E. coli* OP50 off of their bodies.
410 They were then transferred to the PA14 containing plates and incubated at 25°C. The
411 animals were scored every 12 hours until all animals were dead. At least 75 animals
412 were used in each experimental condition.

413 **Heat stress survival assay**

414 Day 1 synchronized *C. elegans* were transferred to fresh NGM plates seeded with
415 *E. coli* OP50. These plates were transferred to a 35°C incubator, where they were
416 evenly distributed throughout the incubator to ensure even heat exposure. The plates
417 were scored for live worms every 2 hours until all of the worms were dead. 20 to 50
418 animals were used in each experimental condition.

419 **Sample collection and RNA purification for sequencing**

420 For RNA sequencing we used day one adults that were hatched within one hour. To
421 achieve this synchronization, we washed all adults and larvae of plates with M9 and
422 allowed the eggs on hatch for one hour. The freshly hatched L1 larvae were then
423 washed off and transferred to fresh plates seeded with OP50 and incubated at 20°C

424 until they developed to adults. At day one of adulthood, animals were washed from
425 their plates and transferred to either control or TM containing plates, where they were
426 incubated for 6 hours. The animals were then washed off using M9 and snap frozen in
427 trizol. All biological replicates were collected and prepared using a snaking collection
428 method to reduce batch effects. Total RNA was purified using Zymo Research Direct-
429 zol RNA Microprep kit.

430 **RNA-seq library preparation**

431 RNA quality was assessed using Agilent's Bioanalyzer platform, and samples with RIN
432 > 9 were used for library construction. 2.5 µg of total RNA was subjected to ribosomal
433 RNA (rRNA) depletion using the Illumina's Ribo-zero Gold kit (Illumina), according to
434 the manufacturer's protocol. Strand specific RNA-seq libraries were then constructed
435 using the SMARTer Stranded RNA-Seq HT Kit (Clontech #634839), according to the
436 manufacturer's protocol. Based on rRNA-depleted input amount, 15 cycles of
437 amplification were performed to generate RNA-seq libraries. Paired-end 150 bp reads
438 were sent for sequencing on the Illumina HiSeq-Xten platform at the Novogene
439 Corporation (USA). The resulting data was then analyzed with a standardized RNA-
440 seq data analysis pipeline (described below).

441 **RNA-seq analysis pipeline**

442 cDNA sequences of worm genes were obtained through ENSEMBL Biomart for the
443 WBCel235 build of the *C. elegans* genome (Ensemble release v94; accessed 2018-
444 12-03). Trimmed reads were mapped to this reference using kallisto 0.43.0-1 and the
445 –fr-stranded option (Bray et al., 2016). All subsequent analyses were performed in the
446 R statistical software (https://cran.r-project.org/). Read counts were imported into R,
447 and summarized at the gene level. Differential gene expression was estimated using

448 the ‘DESeq2’ R package (DESeq2 1.16.1) (Love et al., 2014). DAVID analysis (version
449 6.8) was performed to identify significantly enriched gene ontology terms.

450 **Developmental verapamil resistance assay and lifespan analysis**

451 Plates containing 10 µg/mL TM were supplemented with 1 nM verapamil by adding
452 verapamil solved in DMSO onto the plates. Plates were allowed to dry for 6h before
453 eggs were transferred to them to determine developmental resistance to TM. Plates
454 were then scored after 4 days to determine the relative number of L4 larvae or adults.
455 Lifespan assays were performed as above, however the animals were transferred to
456 fresh verapamil containing plates every second day for the whole lifespan assay. 20 to
457 50 animals were used in each experimental condition.

458 **Data availability**

459 Raw sequencing data were deposited to the NCBI Gene Expression Omnibus (GEO)

460 under the accession number GSE144675.

461

462 **References**

463 ABALLAY, A. 2013. Role of the nervous system in the control of proteostasis during innate
464 immune activation: insights from C. elegans. *PLoS Pathog,* 9**,** e1003433.
465 AFSCHAR, S., TOIVONEN, J. M., HOFFMANN, J. M., TAIN, L. S., WIESER, D., FINLAYSON, A. J.,
466 DRIEGE, Y., ALIC, N., EMRAN, S., STINN, J., FROEHLICH, J., PIPER, M. D. & PARTRIDGE,
467 L. 2016. Nuclear hormone receptor DHR96 mediates the resistance to xenobiotics but
468 not the increased lifespan of insulin-mutant Drosophila. *Proc Natl Acad Sci U S A,*
469 113**,** 1321-6.
470 APFELD, J. & KENYON, C. 1999. Regulation of lifespan by sensory perception in
471 Caenorhabditis elegans. *Nature,* 402**,** 804-9.
472 ARDELLI, B. F. & PRICHARD, R. K. 2013. Inhibition of P-glycoprotein enhances sensitivity of
473 Caenorhabditis elegans to ivermectin. *Vet Parasitol,* 191**,** 264-75.
474 BARGMANN, C. I. 2006. Chemosensation in C. elegans. *WormBook***,** 1-29.
475 BRAY, N. L., PIMENTEL, H., MELSTED, P. & PACHTER, L. 2016. Near-optimal probabilistic RNA-
476 seq quantification. *Nat Biotechnol,* 34**,** 525-7.
477 BRENNER, S. 1974. The genetics of Caenorhabditis elegans. *Genetics,* 77**,** 71-94.
478 BURG, R. W., MILLER, B. M., BAKER, E. E., BIRNBAUM, J., CURRIE, S. A., HARTMAN, R., KONG,
479 Y. L., MONAGHAN, R. L., OLSON, G., PUTTER, I., TUNAC, J. B., WALLICK, H., STAPLEY,
480 E. O., OIWA, R. & OMURA, S. 1979. Avermectins, new family of potent anthelmintic
481 agents: producing organism and fermentation. *Antimicrob Agents Chemother,* 15**,**
482 361-7.
483 CASTELLO, P. R., DRECHSEL, D. A. & PATEL, M. 2007. Mitochondria are a major source of
484 paraquat-induced reactive oxygen species production in the brain. *J Biol Chem,* 282**,**
485 14186-93.
486 COLLINS, J. J., EVASON, K., PICKETT, C. L., SCHNEIDER, D. L. & KORNFELD, K. 2008. The
487 anticonvulsant ethosuximide disrupts sensory function to extend C. elegans lifespan.
488 *PLoS Genet,* 4**,** e1000230.
489 DENT, J. A., SMITH, M. M., VASSILATIS, D. K. & AVERY, L. 2000. The genetics of ivermectin
490 resistance in Caenorhabditis elegans. *Proc Natl Acad Sci U S A,* 97**,** 2674-9.
491 DENZEL, M. S. & ANTEBI, A. 2015. Hexosamine pathway and (ER) protein quality control. *Curr*
492 *Opin Cell Biol,* 33**,** 14-8.
493 DENZEL, M. S., STORM, N. J., GUTSCHMIDT, A., BADDI, R., HINZE, Y., JAROSCH, E., SOMMER,
494 T., HOPPE, T. & ANTEBI, A. 2014. Hexosamine pathway metabolites enhance protein
495 quality control and prolong life. *Cell,* 156**,** 1167-1178.
496 FUJII, M., MATSUMOTO, Y., TANAKA, N., MIKI, K., SUZUKI, T., ISHII, N. & AYUSAWA, D. 2004.
497 Mutations in chemosensory cilia cause resistance to paraquat in nematode
498 Caenorhabditis elegans. *J Biol Chem,* 279**,** 20277-82.
499 GAGLIA, M. M., JEONG, D. E., RYU, E. A., LEE, D., KENYON, C. & LEE, S. J. 2012. Genes that act
500 downstream of sensory neurons to influence longevity, dauer formation, and
501 pathogen responses in Caenorhabditis elegans. *PLoS Genet,* 8**,** e1003133.
502 GEMS, D. & MCELWEE, J. J. 2005. Broad spectrum detoxification: the major longevity
503 assurance process regulated by insulin/IGF-1 signaling? *Mech Ageing Dev,* 126**,** 381-7.
504 HAMPTON, R. Y., GARDNER, R. G. & RINE, J. 1996. Role of 26S proteasome and HRD genes in
505 the degradation of 3-hydroxy-3-methylglutaryl-CoA reductase, an integral
506 endoplasmic reticulum membrane protein. *Mol Biol Cell,* 7**,** 2029-44.

507 HASKINS, K. A., RUSSELL, J. F., GADDIS, N., DRESSMAN, H. K. & ABALLAY, A. 2008. Unfolded
508 protein response genes regulated by CED-1 are required for Caenorhabditis elegans
509 innate immunity. *Dev Cell,* 15**,** 87-97.
510 HEIFETZ, A., KEENAN, R. W. & ELBEIN, A. D. 1979. Mechanism of action of tunicamycin on
511 the UDP-GlcNAc:dolichyl-phosphate Glc-NAc-1-phosphate transferase. *Biochemistry,*
512 18**,** 2186-92.
513 HENIS-KORENBLIT, S., ZHANG, P., HANSEN, M., MCCORMICK, M., LEE, S. J., CARY, M. &
514 KENYON, C. 2010. Insulin/IGF-1 signaling mutants reprogram ER stress response
515 regulators to promote longevity. *Proc Natl Acad Sci U S A,* 107**,** 9730-5.
516 INGLIS, P. N., OU, G., LEROUX, M. R. & SCHOLEY, J. M. 2007. The sensory cilia of
517 Caenorhabditis elegans. *WormBook***,** 1-22.
518 KYRIAKAKIS, E., CHARMPILAS, N. & TAVERNARAKIS, N. 2017. Differential adiponectin
519 signalling couples ER stress with lipid metabolism to modulate ageing in C. elegans.
520 *Sci Rep,* 7**,** 5115.
521 LABBADIA, J. & MORIMOTO, R. I. 2014. Proteostasis and longevity: when does aging really
522 begin? *F1000Prime Rep,* 6**,** 7.
523 LEHNE, G. 2000. P-glycoprotein as a drug target in the treatment of multidrug resistant
524 cancer. *Curr Drug Targets,* 1**,** 85-99.
525 LIBERT, S., ZWIENER, J., CHU, X., VANVOORHIES, W., ROMAN, G. & PLETCHER, S. D. 2007.
526 Regulation of Drosophila life span by olfaction and food-derived odors. *Science,* 315**,**
527 1133-7.
528 LINCKE, C. R., BROEKS, A., THE, I., PLASTERK, R. H. & BORST, P. 1993. The expression of two
529 P-glycoprotein (pgp) genes in transgenic Caenorhabditis elegans is confined to
530 intestinal cells. *EMBO J,* 12**,** 1615-20.
531 LINDBLOM, T. H., PIERCE, G. J. & SLUDER, A. E. 2001. A C. elegans orphan nuclear receptor
532 contributes to xenobiotic resistance. *Curr Biol,* 11**,** 864-8.
533 LOPEZ-OTIN, C., BLASCO, M. A., PARTRIDGE, L., SERRANO, M. & KROEMER, G. 2013. The
534 hallmarks of aging. *Cell,* 153**,** 1194-217.
535 LOVE, M. I., HUBER, W. & ANDERS, S. 2014. Moderated estimation of fold change and
536 dispersion for RNA-seq data with DESeq2. *Genome Biol,* 15**,** 550.
537 MAGNER, D. B., WOLLAM, J., SHEN, Y., HOPPE, C., LI, D., LATZA, C., ROTTIERS, V., HUTTER, H.
538 & ANTEBI, A. 2013. The NHR-8 nuclear receptor regulates cholesterol and bile acid
539 homeostasis in C. elegans. *Cell Metab,* 18**,** 212-24.
540 MATAI, L., SARKAR, G. C., CHAMOLI, M., MALIK, Y., KUMAR, S. S., RAUTELA, U., JANA, N. R.,
541 CHAKRABORTY, K. & MUKHOPADHYAY, A. 2019. Dietary restriction improves
542 proteostasis and increases life span through endoplasmic reticulum hormesis. *Proc*
543 *Natl Acad Sci U S A,* 116**,** 17383-17392.
544 MEISEL, J. D., PANDA, O., MAHANTI, P., SCHROEDER, F. C. & KIM, D. H. 2014.
545 Chemosensation of bacterial secondary metabolites modulates neuroendocrine
546 signaling and behavior of C. elegans. *Cell,* 159**,** 267-80.
547 MENEZ, C., ALBERICH, M., COURTOT, E., GUEGNARD, F., BLANCHARD, A., AGUILANIU, H. &
548 LESPINE, A. 2019. The transcription factor NHR-8: A new target to increase ivermectin
549 efficacy in nematodes. *PLoS Pathog,* 15**,** e1007598.
550 MENEZ, C., ALBERICH, M., KANSOH, D., BLANCHARD, A. & LESPINE, A. 2016. Acquired
551 Tolerance to Ivermectin and Moxidectin after Drug Selection Pressure in the
552 Nematode Caenorhabditis elegans. *Antimicrob Agents Chemother,* 60**,** 4809-19.

553 PAGE, A. P. 2018. The sensory amphidial structures of Caenorhabditis elegans are involved in
554 macrocyclic lactone uptake and anthelmintic resistance. *Int J Parasitol,* 48**,** 1035-
555 1042.
556 PARODI, A. J. 2000. Role of N-oligosaccharide endoplasmic reticulum processing reactions in
557 glycoprotein folding and degradation. *Biochem J,* 348 Pt 1**,** 1-13.
558 PERENS, E. A. & SHAHAM, S. 2005. C. elegans daf-6 encodes a patched-related protein
559 required for lumen formation. *Dev Cell,* 8**,** 893-906.
560 RICHARDSON, C. E., KOOISTRA, T. & KIM, D. H. 2010. An essential role for XBP-1 in host
561 protection against immune activation in C. elegans. *Nature,* 463**,** 1092-5.
562 RIERA, C. E., TSAOUSIDOU, E., HALLORAN, J., FOLLETT, P., HAHN, O., PEREIRA, M. M. A.,
563 RUUD, L. E., ALBER, J., THARP, K., ANDERSON, C. M., BRONNEKE, H., HAMPEL, B.,
564 FILHO, C. D. M., STAHL, A., BRUNING, J. C. & DILLIN, A. 2017. The Sense of Smell
565 Impacts Metabolic Health and Obesity. *Cell Metab,* 26**,** 198-211 e5.
566 SANGSTER, N. C. 1994. P-glycoproteins in nematodes. *Parasitol Today,* 10**,** 319-22.
567 SHEN, X., ELLIS, R. E., LEE, K., LIU, C. Y., YANG, K., SOLOMON, A., YOSHIDA, H., MORIMOTO,
568 R., KURNIT, D. M., MORI, K. & KAUFMAN, R. J. 2001. Complementary signaling
569 pathways regulate the unfolded protein response and are required for C. elegans
570 development. *Cell,* 107**,** 893-903.
571 SHEPS, J. A., RALPH, S., ZHAO, Z., BAILLIE, D. L. & LING, V. 2004. The ABC transporter gene
572 family of Caenorhabditis elegans has implications for the evolutionary dynamics of
573 multidrug resistance in eukaryotes. *Genome Biol,* 5**,** R15.
574 TAKATSUKI, A., ARIMA, K. & TAMURA, G. 1971. Tunicamycin, a new antibiotic. I. Isolation
575 and characterization of tunicamycin. *J Antibiot (Tokyo),* 24**,** 215-23.
576 TAYLOR, R. C. & DILLIN, A. 2013. XBP-1 is a cell-nonautonomous regulator of stress
577 resistance and longevity. *Cell,* 153**,** 1435-47.
578

579 **Acknowledgements**

580 We thank all M.S.D. laboratory members for lively and helpful discussions. We thank
581 Adam Antebi for valuable comments and for *C. elegans* strains. We thank Seung-Jae
582 Lee for valuable comments on the manuscript. We thank the Caenorhabditis Genetics
583 Center (CGC) for strains. We thank the members of the bioinformatics core facility and
584 the FACS and imaging core facility at MPI AGE. B.A.B was supported by a seed grant
585 from the NAVIGAGE foundation, a generous gift from the Hanson-Thorell Family and
586 the Kathleen Gilmore award in aging biology. M.S.D. was supported by ERC-StG
587 640254, by the Deutsche Forschungsgemeinschaft (DFG, German Research
588 Foundation) - Projektnummer 73111208 - SFB 829, and by the Max Planck Society.

589 **Author contributions**

590 G.A.G, M.J.D and M.S.D designed the project. B.A.B, M.S.D and M.J.D supervised the
591 project. G.A.G, M.J.D, L.E.W, M.G, J.E.D, M.J.A., M.D.H, K.S and F.A.M.C.M
592 performed the genetic, cellular and molecular biology work in *C. elegans*. R.J.L.
593 performed the RNA seq analysis. G.A.G, M.J.D and M.S.D wrote the manuscript.
594 G.A.G and M.J.D prepared the figures.

595 **Competing interests**

596 The authors declare no competing interests.

597

598 **Figures and Figure Legends**

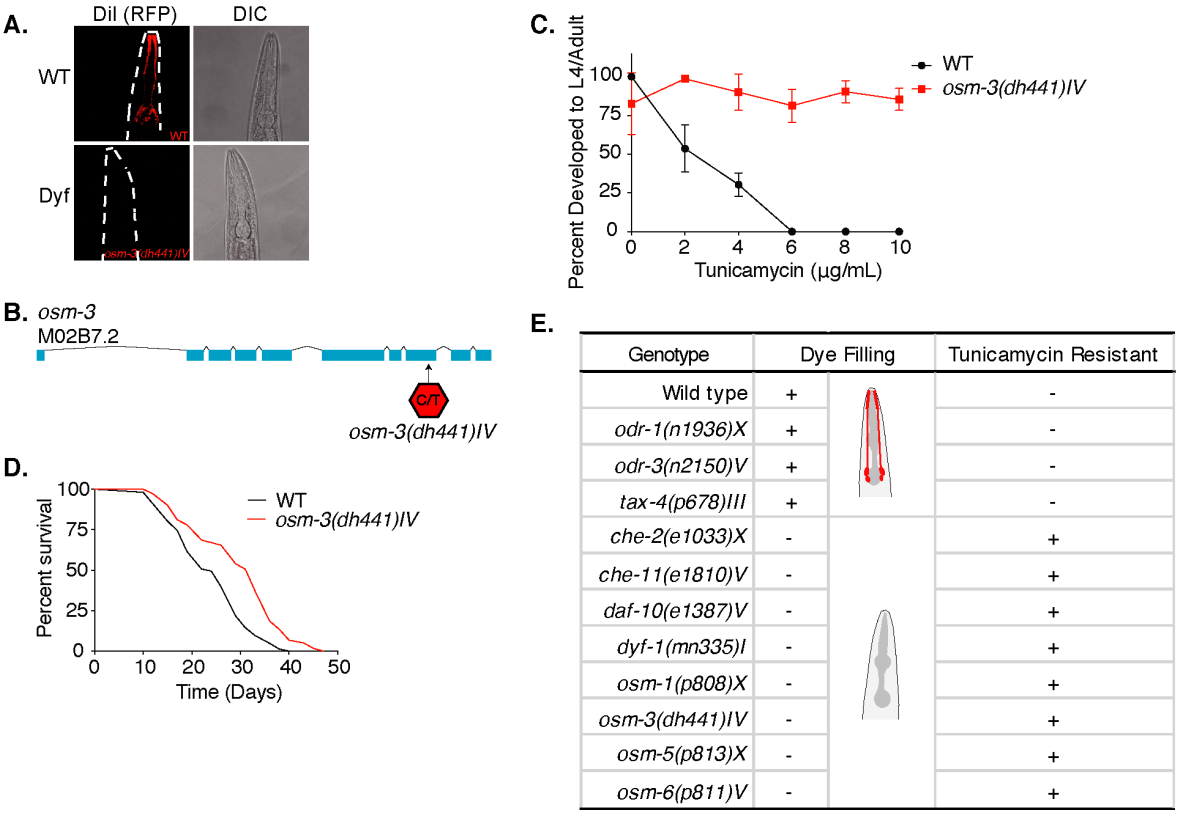

Genotype	Dye Filling		Tunicamycin Resistant
Wild type	+		-
odr-1(n1936)X	+		-
odr-3(n2150)V	+		-
tax-4(p678)III	+		-
che-2(e1033)X	-		+
che-11(e1810)V	-		+
daf-10(e1387)V	-		+
dyf-1(mn335)I	-		+
osm-1(p808)X	-		+
osm-3(dh441)IV	-		+
osm-5(p813)X	-		+
osm-6(p811)V	-		+

599

600 **Figure 1. Tunicamycin resistance occurs in dye filling defective long-lived**
601 **chemosensory *C. elegans* mutants**
602 **A.** Red fluorescence and differential interference contract confocal microscopy images
603 of WT and *osm-3(dh441)IV C. elegans* after DiI treatment.
604 **B.** Depiction of the *osm-3(dh441)* locus. *osm-3(dh441)IV* has a C to T mutation at
605 position 3796925 of exon 8
606 **C.** Developmental tunicamycin (TM) resistance assay using the indicated
607 concentrations with WT and *osm-3(dh441)IV* animals.
608 **D.** Demographic lifespan analysis of WT and *osm-3(dh441)IV* animals. WT mean
609 lifespan = 24 days, *osm-3(dh441)IV* mean lifespan = 29 days, $p<0.0001$.
610 **E.** Table of dye filling phenotype and TM resistance. In the dye filling column, + is
611 positive for DiI filling as in Figure 1A and - is Dyf. In the TM resistant column, + is
612 resistant and - is not resistant to 10 µg/mL TM.

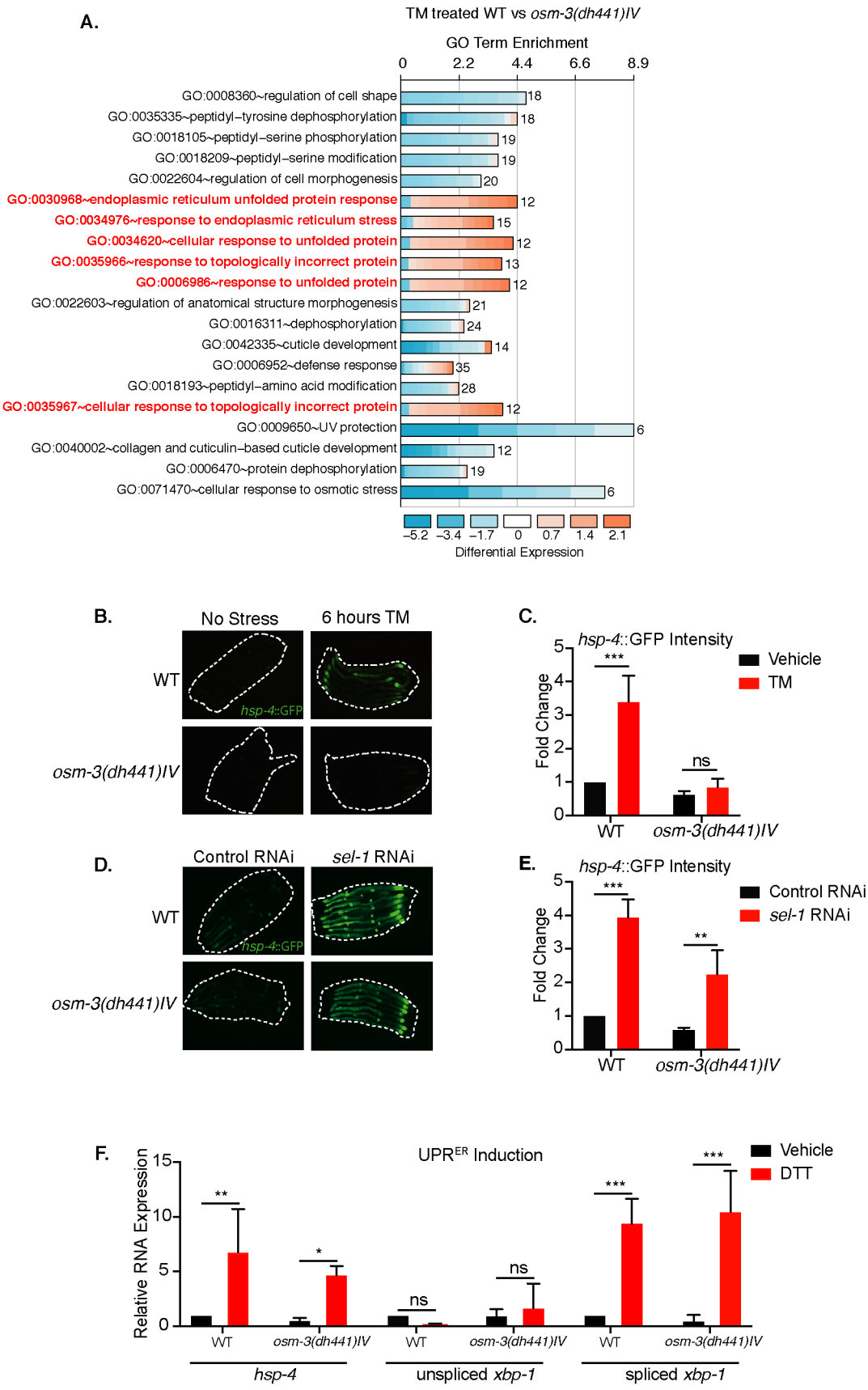

Figure 2. Reduced tunicamycin-induced ER stress signaling in *osm-3* mutants despite functional ER-UPR pathway

A. DAVID gene ontology (GO) terms that are enriched in TM-treated WT compared to TM-treated *osm-3(dh441)IV* worms. Red = upregulated and blue = downregulated.

618 **B.** Green fluorescent images of WT and *osm-3(dh441)IV* animals in the *hsp-4*::GFP
619 reporter background after 6 hours of 10 µg/mL TM treatment. Worms are outlined in
620 the images.
621 **C.** Biosorter analysis of *osm-3(dh441)IV* vs. WT animals in the *hsp-4*::GFP background
622 after 6 hours of control or TM treatment. Data are mean +SEM, n=4, *** $p<0.0001$ by
623 two-way ANOVA.
624 **D.** Green fluorescent images of WT and *osm-3(dh441)IV* animals in the *hsp-4*::GFP
625 background after development on control or *sel-1* RNAi. Worms are outlined in the
626 images.
627 **E.** Biosorter analysis of *osm-3(dh441)IV* vs. WT animals in the *hsp-4*::GFP background
628 raised on control or *sel-1* RNAi. Data are mean +SEM, n=3, ** $p<0.005$ *** $p<0.0001$
629 by two-way ANOVA.
630 **F.** Quantitative PCR measuring relative *hsp-4* and spliced and unspliced *xbp-1* mRNA
631 levels in WT and *osm-3(dh441)IV animals* after 2 hours of 10 mM DTT treatment. Data
632 are mean +SEM, n=3, * $p<0.05$, ** $p<0.001$, *** $p<0.0001$ by two-way ANOVA.

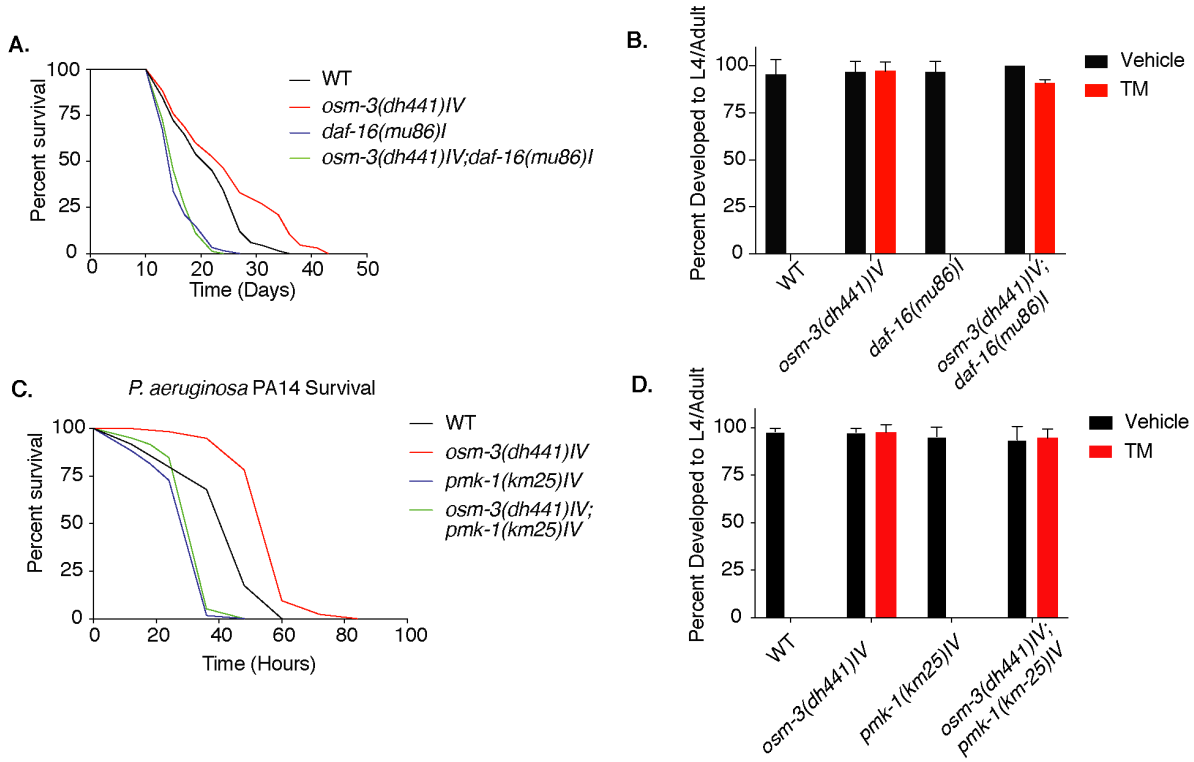

Figure 3. Tunicamycin resistance in *osm-3* mutants is not *daf-16* or *pmk-1* dependent

A. Demographic lifespan analysis of WT, *osm-3(dhh441)IV*, *daf-16(mu86)I* and *osm-3(dh441)IV; daf-16(mu86)I* animals. WT mean lifespan = 22 days, *osm-3(dh441)IV* mean lifespan = 25 days $p<0.005$ compared to WT, *daf-16(mu86)I* mean lifespan = 16 days $p<0.0001$ compared to WT, *osm-3(dh441)IV*; *daf-16(mu86)I* mean lifespan = 16 days $p<0.0001$ compared to WT.

B. Developmental resistance assay using 10 µg/mL TM with WT, *osm-3(dh441) IV*, *daf-16(mu86)I*, and *osm-3(dh441)IV; daf-16(mu86)I* animals.

C. *Pseudomonas aeruginosa* PA14 survival assay with WT, *osm-3(dh441) IV*, *pmk-1(km25)IV*, and *osm-3(dh441)IV; pmk-1(km25)IV* animals. WT mean survival = 44 hours, *osm-3(dh441)IV* mean survival = 58 hours $p<0.001$ compared to WT, *pmk-1(km25)IV* mean survival = 31 hours $p<0.001$ compared to WT, *osm-3(dh441)IV; pmk-1(km25)IV* mean survival = 34 hours $p<0.001$ compared to WT and $p=0.06$ compared to *pmk-1(km25)IV*.

D. Developmental resistance assay using 10 µg/mL TM with WT, *osm-3(dh441)IV*, *pmk-1(km25)IV*, and *osm-3(dh441)IV; pmk-1(km25)IV* animals.

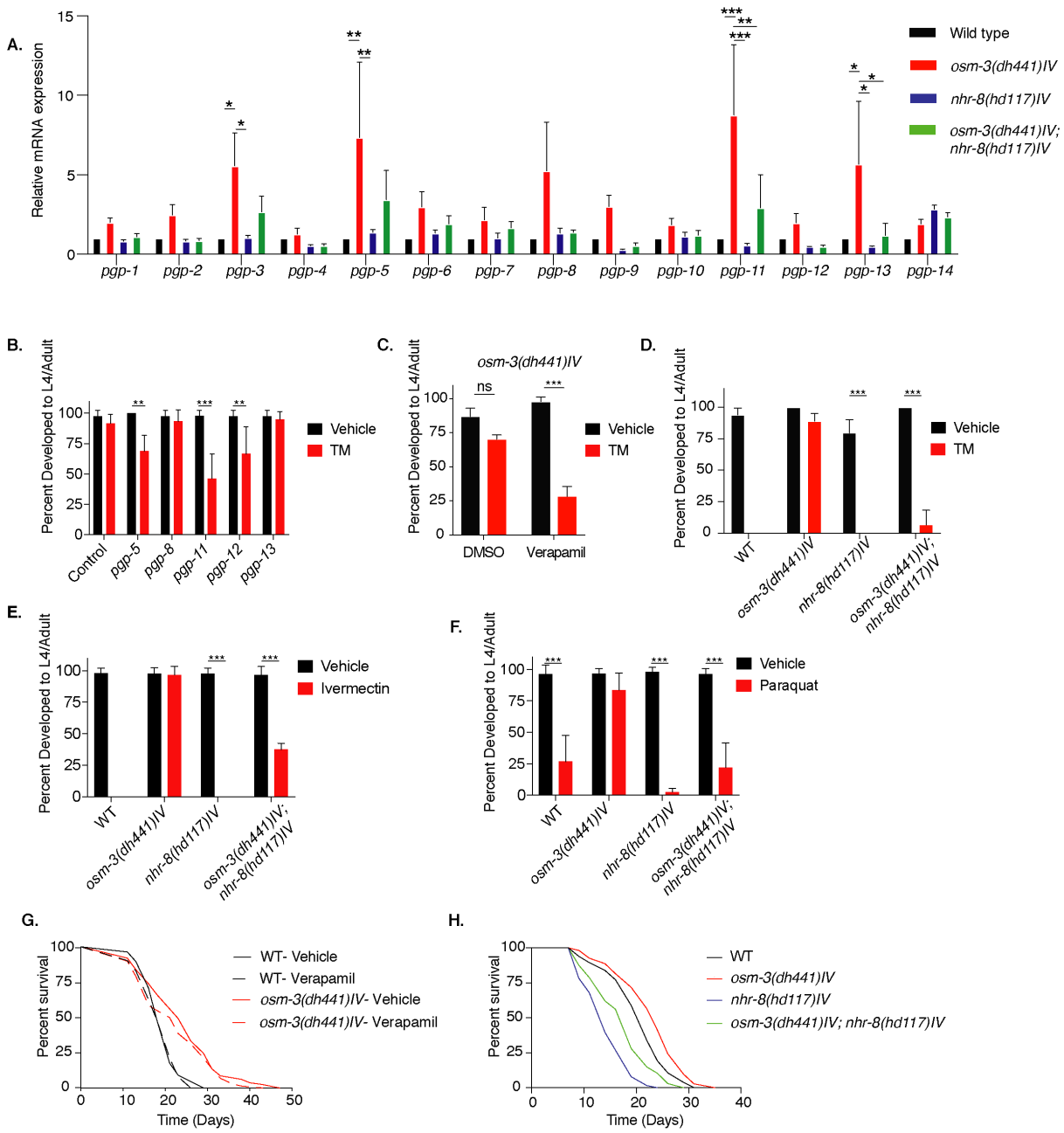

Figure 4. *nhr-8* signaling regulates xenobiotic detoxification response through PGPs

A. Quantitative PCR measuring relative PGP mRNA expression in WT, *osm-3(dh441)IV*, *nhr-8(hd117)IV* and *osm-3(dh441)IV; nhr-8(hd117)IV* animals. Data are mean +SEM, n=3, * p<0.05, ** p<0.001, *** p<0.0001 by two-way ANOVA.

B. Developmental TM resistance assay using 10 µg/mL TM and the indicated RNAi treatments. Data are mean +SD, n=3, ** p < 0.05, *** p<0.001 by two-way ANOVA.

C. Developmental TM resistance assay using the PGP inhibitor verapamil (VPL) using 10 µg/mL TM supplemented with vehicle or 1 nM VPL. Data are mean +SD, n=3, *** p<0.001 by two-way ANOVA.

D. Developmental TM resistance assay on 10 µg/mL TM and control with WT, *osm-3(dh441)IV*, *nhr-8(hd117)IV* and *osm-3(dh441)IV; nhr-8(hd117)IV* animals. Data are mean +SD, n=3, * p<0.05, *** p<0.0001 by t-test.

E. Developmental ivermectin resistance assay of WT, *osm-3(dh441)IV*, *nhr-8(hd117)IV* and *osm-3(dh441)IV; nhr-8(hd117)IV* animals using 6 ng/mL ivermectin and vehicle control. Data are mean +SD, n=3, *** p<0.001 by two-way ANOVA.

F. Developmental paraquat resistance assay of WT, *osm-3(dh441)IV*, *nhr-8(hd117)IV* and *osm-3(dh441)IV; nhr-8(hd117)IV* animals using 0.2 mM paraquat and vehicle control. Data are mean +SD, n=3, *** p<0.001 by two-way ANOVA.

G. Demographic lifespan analysis on vehicle and verapamil treated WT and *osm-3(dh441)IV* worms. Vehicle treated: WT mean lifespan = 19 days; *osm-3(dh441)IV* mean lifespan = 24 days p<0.0001 compared to WT vehicle. verapamil treated: WT mean lifespan = 19 days; *osm-3(dh441)IV* mean lifespan = 22 days, p<0.005 compared to WT Vehicle

H. Demographic lifespan analysis of WT, *osm-3(dh441)IV, nhr-8(hd117)IV and osm-3(dh441)IV;nhr-8(hd117)IV* animals. WT mean lifespan = 22 days, *osm-3(dh441)IV* mean lifespan = 24 days p<0.0001 compared to WT, *nhr-8(hd117)IV* mean lifespan = *14* p<0.0001 compared to WT*, osm-3(dh441)IV; nhr-8(hd117)IV* mean lifespan = 19 days p<0.0001 compared to WT.

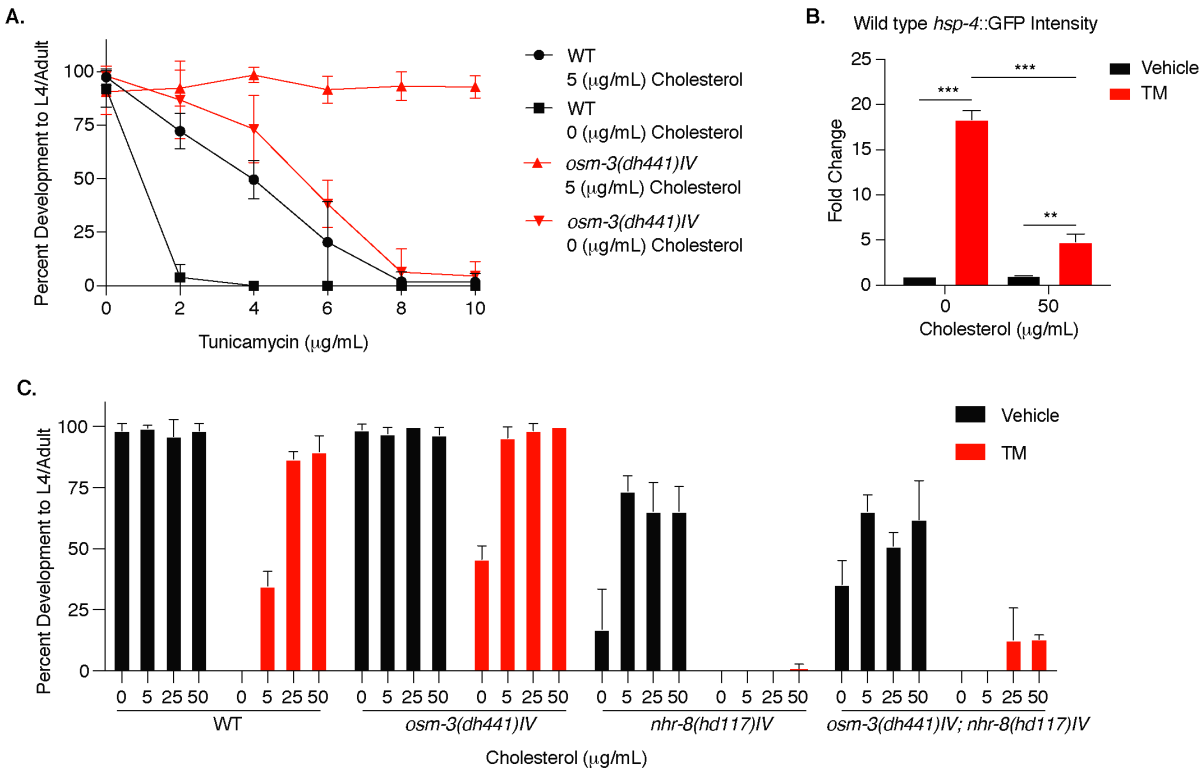

Figure 5. Cholesterol modulates TM resistance through NHR-8

A. Developmental dose response TM resistance assay using the indicated TM concentrations with WT animals and *osm-3(dh441)IV* mutants raised on 0 or 5 μg/mL cholesterol.

B. Biosorter analysis of WT animals with the *hsp-4*::GFP reporter raised on 0 or 50 μg/mL cholesterol after 6 hours of vehicle or 5 μg/mL TM treatment. Data are mean +SEM, n=3, * $p<0.05$, *** $p<0.0001$ by two-way ANOVA.

C. Cholesterol dose response developmental assay with WT, *osm-3(dh441)IV*, *nhr-8(hd117)IV* and *osm-3(dh441)IV; nhr-8(hd117)IV* animals on vehicle or 5 μg/mL TM.

694 **List of Figure supplements**
695 **Figure 1-figure supplement 1.**
696 **Figure 2-figure supplement 1.**
697 **Figure 3-figure supplement 1.**
698 **Figure 4-figure supplement 1.**
699 **Supplementary Table 1**
700 **Supplementary Table 2**
701
702 **List of source data**
703 **Figure 1- source data 1:** Developmental TM resistance assay with WT and *osm-3(dh441)*
704 animals (Fig. 1C)
705
706 **Figure 1-figure supplement 1-source data 1**: Developmental TM resistance assay with WT
707 and *che-2(e1033)X* animals**.** (Figure 1-Fig. Suppl. 1A)
708 **Figure 1-figure supplement 1-source data 2:** Developmental TM resistance assay with WT
709 and *che-11(e1810)V* animals. (Figure 1-Fig. Suppl. 1B)
710 **Figure 1-figure supplement 1-source data 3:** Developmental TM resistance assay with WT
711 and *daf-10(e1387)V* animals. (Figure 1-Fig. Suppl. 1C)
712 **Figure 1-figure supplement 1-source data 4:** Developmental TM resistance assay with WT
713 and *dyf-1(mn335)I* animals. (Figure 1-Fig. Suppl. 1D)
714 **Figure 1-figure supplement 1-source data 5:** Developmental TM resistance assay with WT
715 and *osm-1(p808)X* animals. (Figure 1-Fig. Suppl. 1E)
716 **Figure 1-figure supplement 1-source data 6:** Developmental TM resistance assay with WT
717 and *osm-5(p813)X* animals. (Figure 1-Fig. Suppl. 1F)
718 **Figure 1-figure supplement 1-source data 7:** Developmental TM resistance assay with WT
719 and *osm-6(p811)V* animals. (Figure 1-Fig. Suppl. 1G)
720 **Figure 1-figure supplement 1-source data 8:** Developmental TM resistance assay with WT
721 and *odr-1(n1936)X* animals. (Figure 1-Fig. Suppl. 1H)
722 **Figure 1-figure supplement 1-source data 9:** Developmental TM resistance assay with WT
723 and *odr-3(n2150)V* animals. (Figure 1-Fig. Suppl. 1I)
724 **Figure 1-figure supplement 1-source data 10**: Developmental TM resistance assay with
725 WT and *tax-4(p7689)III* animals. (Figure 1-Fig. Suppl. 1J)
726
727 **Figure 2- source data 1**: Biosorter analysis of *osm-3(dh441)IV* vs. WT animals in the hsp-
728 4::GFP background after 6 hours of control or TM treatment (Fig. 2C)
729 **Figure 2- source data 2**: Biosorter analysis of *osm-3(dh441)IV* vs. WT animals in the hsp-
730 4::GFP background raised on control or *sel-1* RNAi. (Fig. 2E)
731 **Figure 2- source data 3**: Quantitative PCR measuring relative *hsp-4* and spliced and
732 unspliced xbp-1 mRNA levels in WT and *osm-3(dh441)IV* animals after 2 hours of 10 mM
733 DTT treatment (Fig. 2F)
734
735 **Figure 2-figure supplement 1-source data 1:** Quantitative PCR measuring relative mRNA
736 expression of indicated genes in WT animals and *osm-3(dh441)IV* mutants after 6 hours of
737 vehicle or TM treatment
738
739 **Figure 3- source data 1:** Developmental resistance assay using 10 µg/mL TM with WT,
740 *osm-3(dh441)IV, daf-16(mu86)I*, and *osm-3(dh441)IV; daf-16(mu86)I* mutants. (Fig. 3B)
741 **Figure 3- source data 2**: Developmental resistance assay using 10 µg/mL TM with WT,
742 *osm-3(dh441)IV, pmk-1(km25)IV*, and *osm-3(dh441)IV; pmk-1(km25)IV* mutants. (Fig. 3D)
743

744 **Figure 3-figure supplement 1-source data 1:** Biosorter analysis of *osm-3(dh441)IV* vs. WT
745 animals in the *hsp-4*::GFP background raised on control or *daf-16* RNAi. (Figure 3-Fig.
746 Suppl. 3A)
747 **Figure 3-figure supplement 1-source data 2**: Developmental resistance assay using
748 10 µg/mL TM with WT*, osm-3(dh441) IV* and *daf-2(e1370) III* mutants. (Figure 3-Fig. Suppl.
749 3B)
750
751 **Figure 4- source data 1:** Quantitative PCR measuring relative PGP mRNA expression in
752 WT, *osm-3(dh441)IV, nhr-8(hd117)IV* and *osm-3(dh441)IV; nhr-8(hd117)IV* animals (Fig. 4A)
753 **Figure 4- source data 2:** Developmental TM resistance assay using 10 µg/mL TM and the
754 indicated PGPs RNAi treatment. (Fig. 4B)
755 **Figure 4- source data 3:** Developmental TM resistance assay using the PGP inhibitor
756 verapamil (VPL) using 10 µg/mL TM supplemented with vehicle or 1 nM VPL. (Fig. 4C)
757 **Figure 4- source data 4:** Developmental TM resistance assay on 10 µg/mL TM and control
758 with WT, *osm-3(dh441)IV, nhr-8(hd117)IV* and *osm-3(dh441)IV; nhr-8(hd117)IV* animals
759 (Fig. 4D)
760 **Figure 4- source data 5:** Developmental ivermectin resistance assay of WT, *osm-*
761 *3(dh441)IV, nhr-8(hd117)IV* and *osm-3(dh441)IV; nhr-8(hd117)IV* animals using 6 ng/mL
762 ivermectin and vehicle control (Fig. 4E)
763 **Figure 4- source data 6:** Developmental paraquat resistance assay of WT, *osm-3(dh441)IV,*
764 *nhr-8(hd117)IV* and *osm-3(dh441)IV; nhr-8(hd117)IV* animals using 0.2 mM paraquat and
765 vehicle control (Fig. 4F)
766
767 **Figure 4- figure supplement 1-source data 1:** Heat shock assay at 35°C in WT and *osm-*
768 *3(dh441)IV* animals on day 1 of adulthood. (Fig. 4-Fig. Supp.4A)
769 **Figure 4- figure supplement 1-source data 2:** Hydrogen peroxide survival assay using
770 1mM H2O2 on day 1 of adulthood in WT and *osm-3(dh441)IV* animals. (Fig. 4-Fig. Supp.4B)
771 **Figure 4- figure supplement 1-source data 3:** WT development on 0 to 1µM Verapamil.
772 (Fig. 4-Fig. Supp.4C)
773
774 **Figure 5- source data 1**: Developmental dose response TM resistance assay using the
775 indicated TM concentrations with WT animals and *osm-3(dh441)IV* mutants raised on 0 or 5
776 µg/mL cholesterol. (Fig. 5A)
777 **Figure 5- source data 2:** Biosorter analysis of WT animals with the hsp-4::GFP reporter
778 raised on 0 or 50 µg/mL cholesterol after 6 hours of vehicle or 5 µg/mL TM treatment. (Fig.
779 5B)
780 **Figure 5- source data 3:** Cholesterol dose response developmental assay with WT, *osm-*
781 *3(dh441)IV, nhr-8(hd117)IV and osm-3(dh441)IV; nhr-8(hd117)IV* animals on vehicle or
782 5 µg/mL TM. (Fig. 5C)

Figure 1-figure supplement: Tunicamycin resistance occurs in dye filling defective long-lived chemosensory *C. elegans* mutants

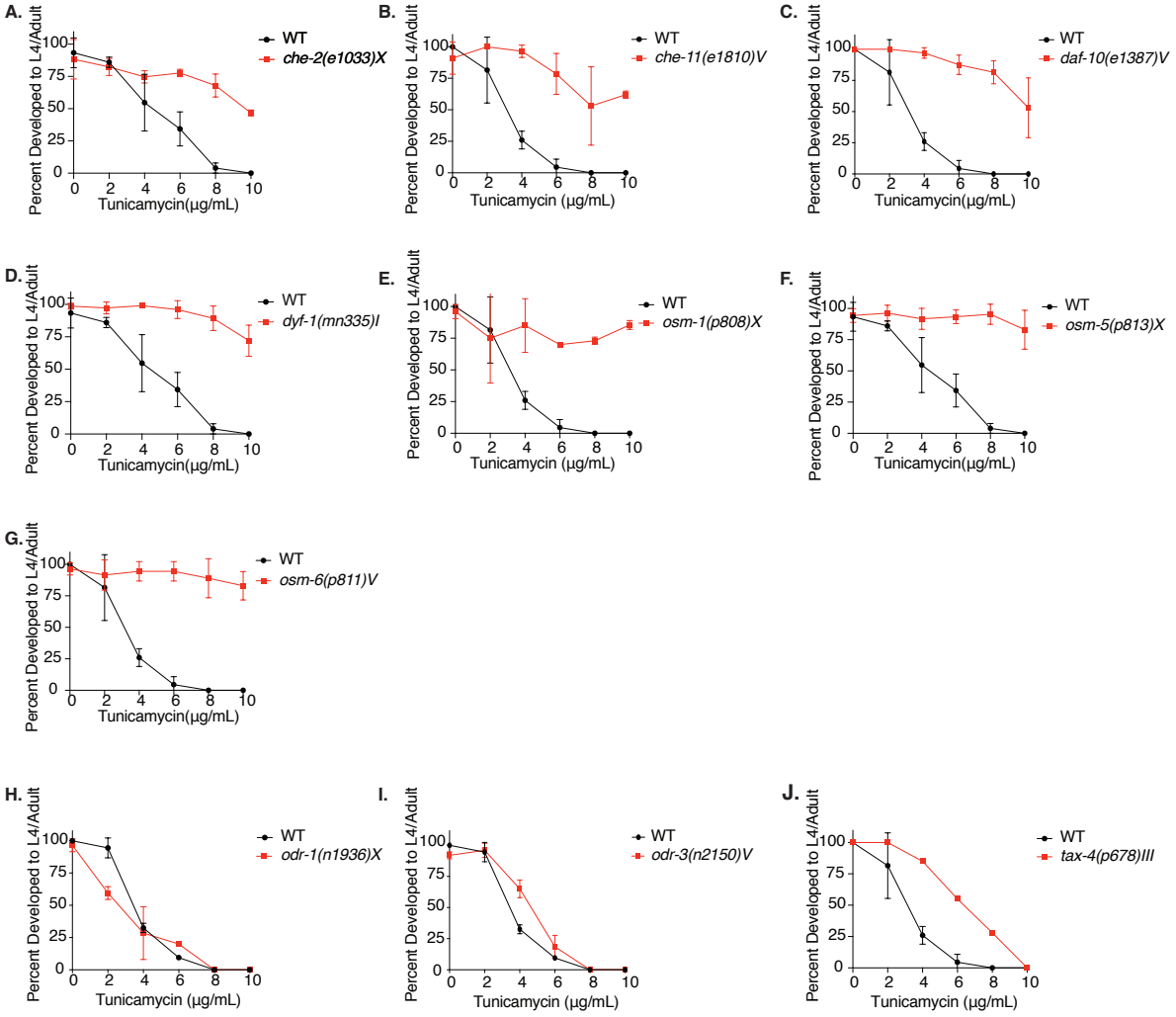

Figure 1-figure supplement 1, A-J. Developmental TM resistance assay with WT, *che-2(e1033)X, che-11(e1810)V*, *daf-10(e1387)V*, *dyf-1(mn335)I, osm-1(p808)X, osm-5(p813)X, osm-6(p811)V, odr-1(n1936)X*, *odr-3(n2150)V* and *tax-4(p678)III* animals.

Figure 2-figure supplement: Reduced tunicamycin-induced ER stress signaling in *osm-3* mutants despite functional ER-UPR pathway

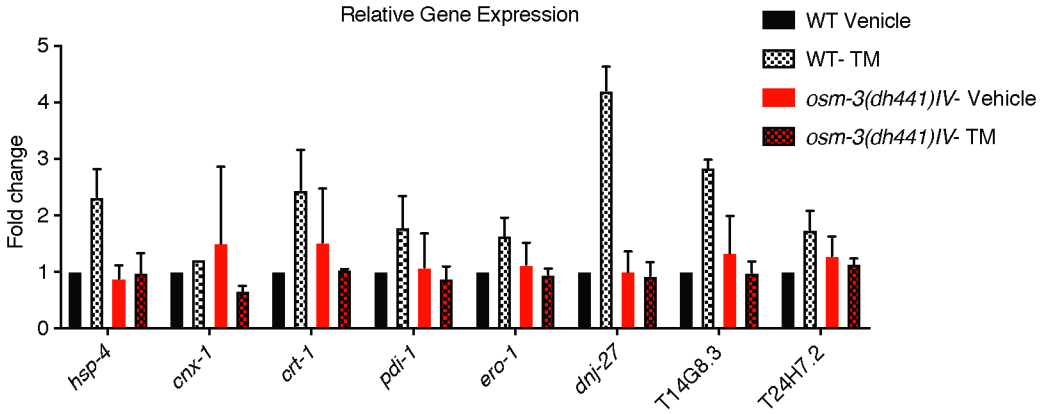

Figure 2-figure supplement, Quantitative PCR measuring relative mRNA expression of indicated genes in WT animals and *osm-3(dh441)IV* mutants after 6 hours of vehicle or TM treatment.

Figure 3-figure supplement: Tunicamycin resistance in *osm-3* mutants is not *daf-16* or *pmk-1* dependent

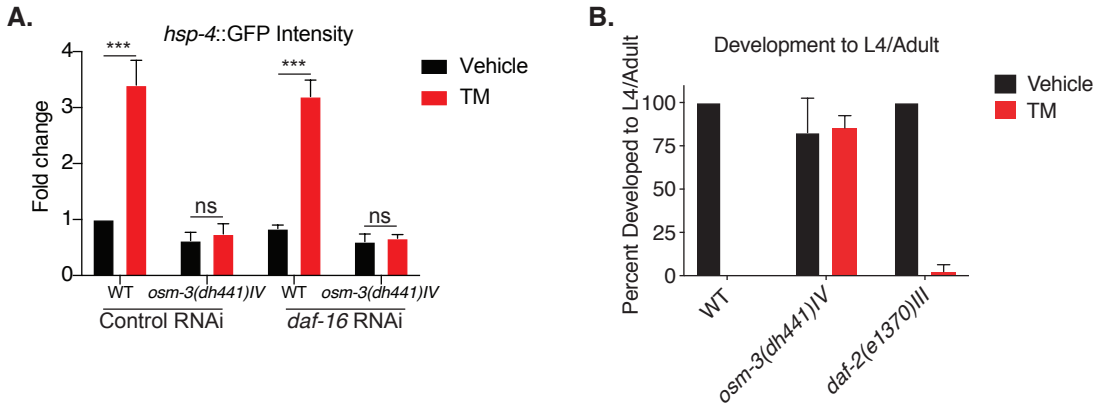

Figure 3-figure supplement, A. Biosorter analysis of *osm-3(dh441)IV* vs. WT animals in the *hsp-4*::GFP background raised on control or *daf-16* RNAi. Data are mean +SEM, n=4, *** p<0.0001 by two-way ANOVA. **B.** Developmental resistance assay using 10 µg/mL TM with WT, *osm-3(dh441)IV* and *daf-2(e1370)III* animals.

Figure 4-figure supplement: *nhr-8* signaling regulates xenobiotic detoxification response through PGPs

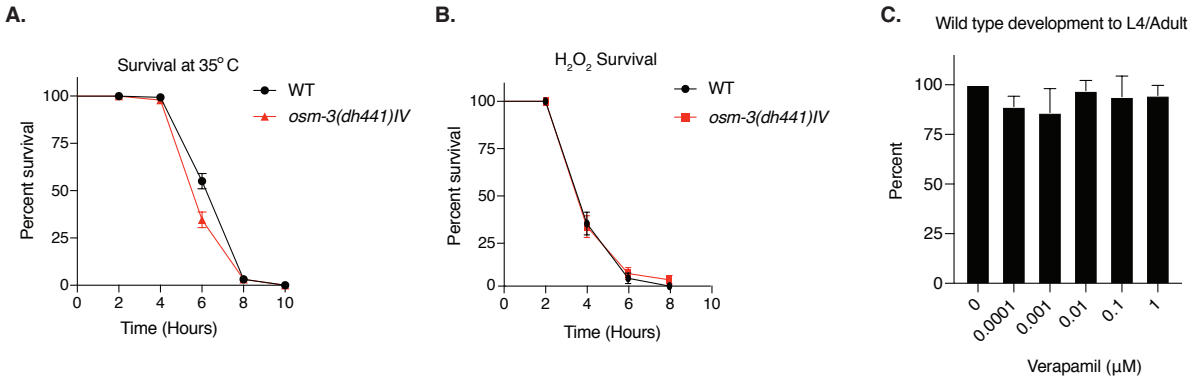

Figure 4-figure supplement, A. Heat shock assay at 35°C in WT and *osm-3(dh441)IV* animals on day 1 of adulthood. WT mean survival = 7 hours, *osm-3(dh441)IV* mean survival = 6 hours, $p<0.01$. **B.** Hydrogen peroxide survival assay using 1 μM H_2O_2 on day 1 of adulthood in WT and *osm-3(dh441)IV* animals. WT mean survival = 7 hours, *osm-3(dh441)IV* mean survival = 6 hours, no significant difference. **C.** WT development on 0 to 1 μM Verapamil. No significant difference in development.